

Hydrociper: Bioinspired Dynamic Structural Color-Based Cryptographic Surface

Jaeho Choi, Mutian Hua, Seung Yeol Lee, Wonhee Jo, Chiao-Yueh Lo, Shin-Hyun Kim,*
Hee-Tak Kim,* and Ximin He*

Structural colors of 2D gratings are iridescent, color-tunable, and never fade, which renders them appealing for anti-counterfeiting applications. However, for advanced security, it still remains a challenge to completely hide the encrypted color patterns and reveal them on demand. In this work, a water-responsive photonic grating consisting of a micropillar array and a hydrogel overcoat with a similar refractive index, termed “hydrociper”, is presented. The joint effect of stimuli-reversible refractive-index (mis)match and reconfigurable grating-based diffraction coloration enables a complete encryption of the structural color and rapid decryption. The photonic structure shows a strong iridescence due to the angle-dependent diffraction when the hydrogel overcoat is swollen from water. Upon drying, the micropillars bend and the refractive index contrast disappears, which dramatically lessens the diffraction intensity and renders the surface highly transparent. The dehydrated-to-hydrated state transition can occur within 1 s, enabling fast decryption. The color switching is highly reversible over a prolonged hydration/dehydration cycle, and the dehydrated hydrogel layer protects the delicate micropillar array from external mechanical stress. The creative combination of hydrogel material and the 2D grating structure offers a new and simple strategy for realizing reversible, durable, and fast-response cryptography with potentially broad impact on the anti-counterfeiting technology market.

interference at a selected wavelength.^[1] The structural colors are usually glittering and iridescent, and they never fade out as long as the structures are maintained. Moreover, they can be varied with a single set of materials by adjusting the periodicity and can be switched off by reducing the refractive index contrast between the structures and the surroundings. These features, distinguished from those of chemical pigments or dyes, make them useful in various optical and photonic applications.^[2] In particular, structural colors are highly attractive for anti-counterfeiting purposes, as they can be hardly duplicated or imitated.^[3]

Micropatterned structures of colloidal crystals and cholesteric liquid crystals have been intensively investigated as a structural motif of anti-counterfeiting tags.^[4] To provide advanced security with cryptographic capabilities, the color patterns should be hidden in the materials (i.e., encryption) and be selectively and dynamically disclosed when a target stimulus is applied (i.e., decryption).^[5] For example, colloidal crystals are embedded in a poly-

meric matrix whose crosslinking density is regioselectively adjusted.^[6] In a similar manner, the crosslinking density of cholesteric liquid crystals is adjusted.^[7] These materials reveal their hidden patterns under mechanical deformation or solvent swelling. However, most conventional photonic systems often present undesirable incomplete encryption.^[5–7] In another approach, the surface wetting property of colloidal crystals or inverse opals has been regioselectively modified for the selective disclosure of the hidden pattern through liquid infiltration or vapor condensation.^[8] However, the complete encryption at hidden state has been still challenging. Recently, bilayer inverse-opal heterostructures have been used to completely encrypt photonic pattern, where the infiltration of ethanol makes one of the inverse-opal layer transparent, which discloses the completely hidden patterns in the other layer.^[9] Even though these approaches enable the complete encryption and facile inspection of authenticity without additional equipment. Nevertheless, it still remains a challenge to completely hide the encrypted color pattern, simplify the fabrication process, make the patches transparent, reduce the production cost, and improve the mechanical stability for practical uses.


1. Introduction

Periodic structures with feature sizes comparable with visible wavelengths develop diffraction colors through constructive

J. Choi, M. Hua, C.-Y. Lo, Prof. X. He
Department of Materials Science and Engineering
University of California
Los Angeles, CA 90095, USA
E-mail: ximinhe@ucla.edu

J. Choi, S. Y. Lee, W. Jo, Prof. S.-H. Kim, Prof. H.-T. Kim
Department of Chemical and Biomolecular Engineering
Korea Advanced Institute of Science and Technology (KAIST)
Daejeon 305-701, Republic of Korea
E-mail: kim.sh@kaist.ac.kr; heetak.kim@kaist.ac.kr

Prof. S.-H. Kim, Prof. H.-T. Kim
KAIST Institute for the NanoCentury
Korea Advanced Institute of Science and Technology
Daejeon 305-701, Republic of Korea

 The ORCID identification number(s) for the author(s) of this article can be found under <https://doi.org/10.1002/adom.201901259>.

DOI: 10.1002/adom.201901259

2D gratings can be a pragmatic alternative to 3D or 1D colloidal crystals and cholesteric liquid crystals for anti-counterfeiting tags.^[10] Although the grating diffraction develops a relatively faint color, it provides a wider viewing angle and higher angle dependency;^[11] 3D and 1D colloidal crystals and cholesteric liquid crystals show bright reflection colors only for specular reflection, at which a blueshift from red to blue requires the change of the angle as large as several tens of degrees.^[12] In addition, the structures can be easily produced by simple micromolding processes such as soft lithography and imprinting.^[13] Due to these advantages, the diffraction gratings with straight line, spiral, and butterfly-like 2D patterns have been employed to develop diffraction colors in the banknote.^[14] Recently, a hexagonal array of hemispherical nanodomains on a flexible polymer substrate was prepared by nanoimprinting and used to develop angle-dependent full rainbow colors.^[15] However, the encryption of a structural color pattern in the grating structure has not been reported to the best of our knowledge. Also, achieving a fast and repeatable decryption of the structural colors from 2D structures has been neither suggested nor attempted.

In this work, we design a water-responsive diffraction grating for the dynamic decryption of encrypted color patterns using a hydrogel-coated micropillar array, termed “hydrociphier” henceforth. Hydrogel is known for the high water affinity and significant changes in volume and optical properties (e.g., refractive index) upon (de)hydration, hence serving as an active component to actuate the passive components to form a water-responsive reconfigurable surface.^[16] Specifically, when the dehydrated hydrogel is exposed to water, the hydrophilic side groups interact strongly with water and in-take water, accompanied by the macroscopic change of swelling (volume expansion). When the hydrated hydrogel is exposed to air the absorbed water will leave the polymer networks due to evaporation, accompanied by the macroscopic change of deswelling (volume reduction). Epoxy is chosen as the passive micropillar material for its decent elasticity to be actuated by the hydrogel and its appropriate refractive index matching that of dry hydrogel for desirable optical transparency in encryption state.^[16] Due to the pillar’s reversibly bendable nature, we specifically chose the micropillar structure for on-demand disruption/restoration of the structure regularity to aid the turn “off”/“on” of the structural color, which was not realized before by using other structures such as periodic opal/inverse opal and thin film structures.^[2c,d,3b,d] The upright micropillar array shows angle-dependent diffraction colors when the hydrogel overcoat is hydrated. As the hydrogel is shrunken upon drying, the micropillars bend down known as a hydrogel “muscle” induced buckling effect,^[16] the structural regularity is reduced and the refractive index of the hydrogel layer closely approaches to that of the micropillars, which render the composite film highly transparent and colorless. Therefore, any graphics or patterns of the micropillar array are completely hidden at the dehydrated state and clearly disclosed at the hydrated state in a reversible manner. The hydration-induced decryption process can be completed within a second due to the rapid hydration kinetics of the thin hydrogel layer. The dehydration-induced encryption can be realized even in ambient condition at room temperature, which is convenient for practical applications. In addition, the

dehydrated overcoat mechanically protects the fragile micropillar array from an external mechanical stress at an encrypted state. The water-responsive encryption and decryption of structural colors are demonstrated, and the working principles are explored.

2. Results and Discussion

2.1. Fabrication of Hydrogel-Coated Micropillar Array

The hydrociphier based on a hydrogel-coated micropillar array is fabricated by (i) preparing a micropillar array through soft-molding the epoxy resin with a microhole array-containing the polydimethylsiloxane (PDMS) mold and (ii) casting an in situ polymerized hydrogel overcoat on the micropillar array, as schematically illustrated in **Figure 1a**. The PDMS mold, which has a predefined pattern of a square array with cylindrical microholes that have a diameter of 1 μm , a depth of 3 μm , and a hole-to-hole distance of 2 μm , was prepared by combining soft-molding and photolithography (Figure S1, Supporting Information). In the first process, an epoxy resin containing glycidyl methacrylate was dropped on a glass substrate, the surface of which was functionalized with 3-(trimethoxysilyl)propyl methacrylate (TMSPMA).^[16] The PDMS mold was also placed on the epoxy resin cast. The epoxy resin readily filled the microholes of the PDMS mold by capillary force. After curing the epoxy resin by UV irradiation, the PDMS mold was gently released. The resulted dimensions of the micropillar array were equivalent to those of the microholes in the PDMS mold, as confirmed by scanning electron microscopy (SEM) analysis (Figure S2, Supporting Information). Using the method, a “K” pattern composed of a square array of micropillars was prepared, as shown in the insets of Figure 1a. In the second process, a poly(acrylamide) (PAAm) hydrogel precursor, which is a mixture of acrylamide and water with a weight ratio of 1:10 containing a crosslinker and a photoinitiator, was dropped on the micropillar array, followed by covering with a glass slide, and irradiating UV. As a result, the water-swollen PAAm hydrogel occupied the interstitial spaces among the straight micropillars and formed a top layer on the micropillar array. The methacrylate moieties in the epoxy resin covalently bond the PAAm hydrogel overcoat with the epoxy micropillar array, which is a key to enabling the hydrogel “muscle” (de)swelling to effectively induce pillar (de)bending. Such a design allows for large-scale production via 3D printing or a roll-to-roll process consisting of pattern imprinting and UV curing of the hydrogel coating.

2.2. Encryption and Decryption of Color Patterns

To investigate the structure of the hydrociphier at the swollen state, the as-prepared hydrated sample was freeze-dried and subjected to SEM investigation. As shown in Figure 1b, the straight micropillar array was buried in the hydrogel overcoat. As the refractive index of the polymerized epoxy resin ($n_e \approx 1.51$) was larger than the water-swollen hydrogel ($n_{\text{hyd}} \approx 1.33$), the square array of the micropillars diffracted light, rendering the patterns iridescent.^[17] This was demonstrated by the letters

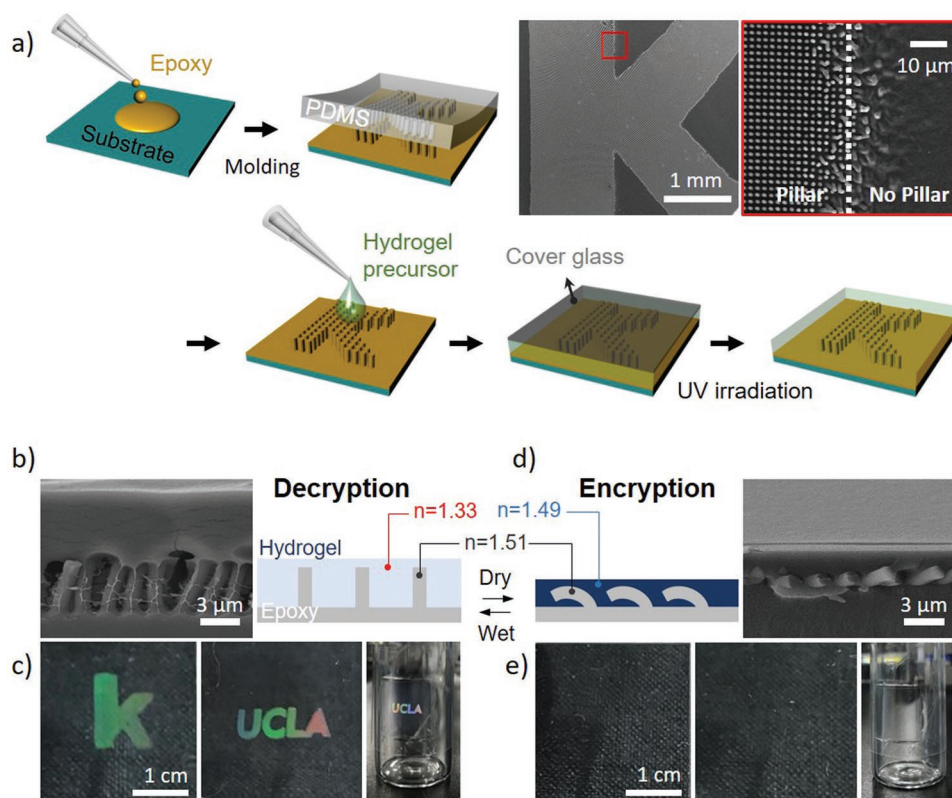


Figure 1. a) The design and fabrication procedure of hydrociphier based on a hydrogel-coated micropillar pattern. The insets are SEM images of a pattern composed of square array of micropillars that constitute “K.” b) Cross-sectional SEM images and the schematic of the as-prepared hydrociphier at a hydrated state. The sample for SEM measurement was prepared by freeze-drying the hydrated hydrociphier with the morphology of swollen hydrogel well preserved. c) Images of two different color patterns of “K” “UCLA” at their hydrated state. d) Cross-sectional SEM images and the schematic of the dehydrated hydrociphier. e) The disappearance of the color patterns shown in (c) after drying.

“K” and “UCLA” pattern shown in Figure 1c. It is worth noting that the hydrociphier can be prepared on a flexible polyethylene terephthalate (PET) substrate, which is bendable and applicable on curved surfaces (Figure 1c).

As the hydrogel overcoat was air-dried in ambient environment, the hydrogel layer was shrunk along the thickness direction, which was accompanied by the bending of the micropillars shown in Figure 1d. Interestingly, the micropillar array became highly transparent without any apparent diffraction colors after drying, as shown in Figure 1e, indicating the encryption of the color patterns. The drastic transition to a transparent state with dehydration has two different origins. Since the refractive index of the dehydrated PAAm ($n_{\text{dehyd}} \approx 1.49$) is quite closer to that of the micropillars ($n_e \approx 1.51$), compared to that of the hydrated PAAm ($n_{\text{hyd}} \approx 1.33$), the refractive index contrast is lowered, and the diffraction is lessened with drying.^[18] However, the refractive index contrast cannot be completely removed due to the small difference in the refractive index ($n_e - n_{\text{dehyd}} = 0.02$), which suggests the existence of the other mechanism. As well as the decreased refractive index contrast, the bending of the micropillars with drying can also contribute to the transparency.^[19] This lowers the regularity of the square array and the height of the diffraction structures. In addition, the bending makes a gradient of the effective refractive index between the

dehydrated PAAm and micropillars, thereby diminishing the scattering intensity in a similar manner to the antireflection coatings. To verify the structural effect, a hydrogel overcoat with a lower deswelling ratio was fabricated using the precursor solution with a lower water content (acrylamide/water = 1/1 in weight). Due to a smaller volume contraction of such a hydrogel upon drying, the bending of the micropillars was less significant. As shown in Figure S3 (Supporting Information), even after drying, the film with less bent pillars in the low-deswelling-ratio hydrogel still exhibited a weak diffraction color. This indicates that the bending of micropillars is a critical element to the hiding of the diffraction colors as well as the refractive index matching.

The original color patterns were quickly recovered by dropping water on the dried pattern, as shown in Movie S1 (Supporting Information). In line with the structural effect on the dehydration-induced encryption, the erection of the bent micropillars by hydration is important for achieving a full recovery of the original color patterns. To study the importance of the upright configuration, a bent micropillar array was fabricated by dropping water on the straight micropillar and placing a glass slide on top of the micropillar. During the evaporation of the water trapped between the slides, the pillars collapsed, resulting in the bent micropillar array shown in Figure S4a (Supporting Information). Then the hydrogel layer was formed

on the bent micropillar arrays. The resulting hydrogel/bent-micropillar array composite displayed diffraction colors at a fully hydrated state. However, those colors were much weaker than those from the straight micropillar structures, as shown in Figure S4b (Supporting Information). The observation again demonstrates that the shape transformation is one of the key principles for realizing the drastic color switching. Thus, the two factors—structural and refractive index—are both indispensable; they act synergistically in achieving high cryptographic performance owning complete encryption and clear decryption.

2.3. Mechanical Robustness of the Encryption Surface

Protecting the encrypted color pattern from external mechanical stresses is of great importance for practical anti-counterfeit applications. In this aspect, the solid overcoat serves as a protective layer for the delicate micropillar array against abrasion or dust accumulation in real-life environment. At room temperature in ambient condition, the dehydrated PAAM is in its glassy state, and its compression modulus is as high as 5 GPa.^[20] Nanoindentation test to the surface of hydrociphier also provided elastic modulus as high as 9 GPa (Figure S5, Supporting Information). Therefore, under a normal level of mechanical stress such as manual pressing and rubbing, the PAAM layer

can protect the array. As demonstrated in Movie S2 (Supporting Information), after pressing and rubbing the hydrociphier repetitively, the decryption of the encrypted color pattern upon hydration could still be successfully achieved. In addition, the hydrociphier remains undamaged and exhibits decryption of the color patterns after holding at high temperature of 150 °C for 3 h, which ensures thermal stability of the hydrociphier. In general, such a platform is anticipated to be stable at most of ambient conditions below the glass-transition temperatures of the gels used (e.g., reported range 153–225 °C for PAAm).^[21]

2.4. Optical Properties at Decrypted and Encrypted States

The diffraction color from the hydrated hydrociphier varies with the angles of incident light and observation, which is not achievable with chemical pigments and is beneficial for anti-counterfeiting applications. The angle dependence was investigated by measuring the reflectance of the hydrated hydrociphier, the grating vector of which was oriented to be on the plane of incidence ($\varphi = 0^\circ$). At a fixed reflection angle (θ_d) of 30° , the peak position shifted from 623 to 493 nm as the incident light (θ_i) increased from 11° to 15° , as shown in Figure 2a, where the absolute reflectivity is measured to be $\approx 0.3\%$ as shown in Figure S6 (Supporting Information).^[10a] From the responses,

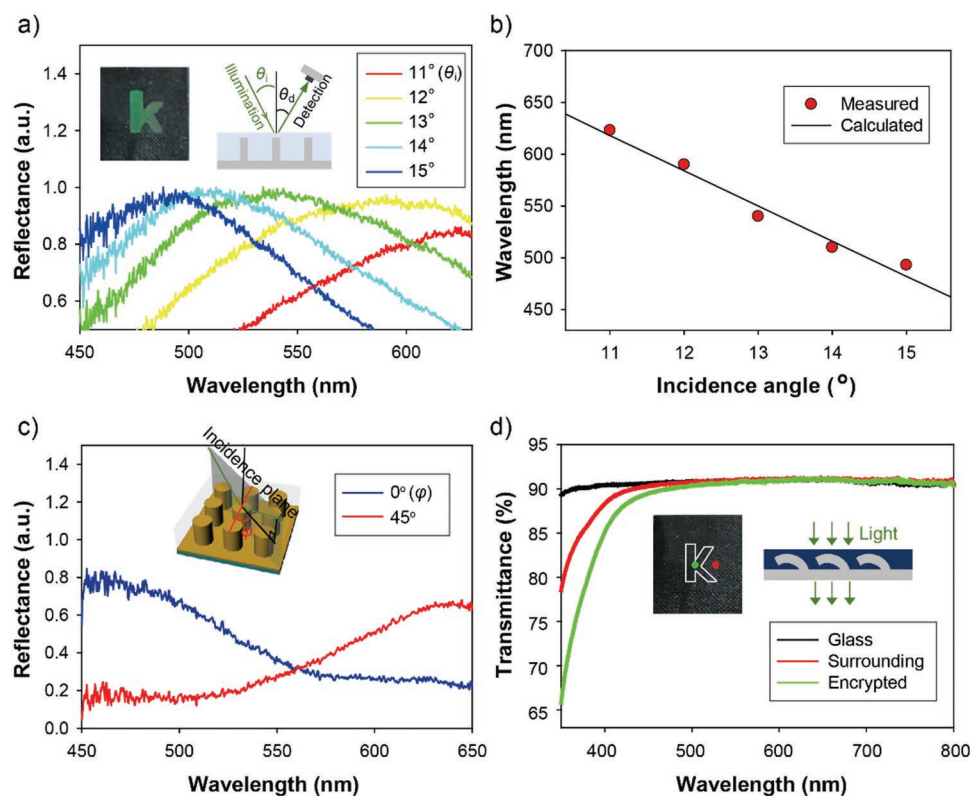


Figure 2. a) Normalized reflectance spectra taken along the axis of square array of micropillars at a hydrated state, where the angle of incident white light, θ_i , is varied from 11° to 15° while setting the angle of detection to $\theta_d = 30^\circ$. b) Diffraction wavelength as a function of θ . The dotted line indicates the diffraction wavelength calculated from the first-order grating diffraction. c) Reflectance spectra taken along the axis ($\varphi = 0^\circ$) and diagonal ($\varphi = 45^\circ$) of the square array, where $\theta_i = 16^\circ$ and $\theta_d = 30^\circ$. d) Transmittance spectra for the pattern and nonpattern regions on a hydrociphier, that is, the hydrogel-coated micropillar pattern area (green line) and a plain hydrogel film area formed on epoxy-coated glass (red line) at their dried state, and a bare glass substrate (black line).

it can be verified whether the micropillar array was preserved after the formation of the hydrogel overcoat. The wavelength for constructive interference is known to follow the grating diffraction equation

$$m\lambda = d|\sin\theta_i - \sin\theta_d| \quad (1)$$

where m is a diffraction order and d is the center-to-center distance between two adjacent micropillars along the direction of the incident light and observation. The angle-dependent change of the reflectance peak, $\lambda(\theta_i)$, is in good agreement with Equation (1) for the first-order diffraction ($m = 1$) and $d = 2 \mu\text{m}$, as shown in Figure 2b. When the sample was rotated by 45° as to position the diagonal direction of the square array on the incidence plane ($\varphi = 45^\circ$), the diffraction wavelength shifted from 455 nm ($\varphi = 0^\circ$) to 638 nm ($\varphi = 45^\circ$) due to the increase of d from 2.0 to 2.8 μm , as shown in Figure 2c. The result is also consistent with the theoretical calculation using Equation (1). Therefore, the hydrogel overcoat does not distort the original structural color. A practical implication from the observation is that the structural color can be designed simply by adjusting the diffraction structure of 2D grating. With this useful design tool based on the governing equation, more complex multicolor patterns can be realized.

The diffraction colors completely disappeared when the film was fully dried. The array of bent micropillars buried in the dehydrated PAAm layer did not make any optical contrast

to the micropillar-free background for naked eyes. For more quantitative analysis, the transmission spectra for the dehydrated hydrociphher and dehydrated hydrogel film formed on the epoxy-coated glass substrate were taken and compared with that for the glass substrate. As shown in Figure 2d, the transmittances for the dehydrated hydrociphher were not different from those for the dehydrated hydrogel film and the glass substrate above 500 nm. They were as high as 90%, verifying the complete encryption of the structural colors and transparency. The lowered transmittances below 500 nm for the films were attributed to the absorption of the epoxy and PAAm materials. Also, the dehydrated hydrociphher did not show any haze when it was placed on a black-colored surface, as shown in the inset of Figure 2d.

2.5. Decryption Speed

Understanding the mechanism for recovering the original color with hydration and the key factors affecting the response time is very important for the rapid inspection of authenticity in anti-counterfeiting applications. To quantitatively study the dynamic water-sensitive coloring, we monitored the evolution of the reflectance spectra of the 3 μm thick hydrogel-coated micropillar array (denoted as 3 μm thick hydrociphher) at $\varphi = 0^\circ$, $\theta_i = 13^\circ$, and $\theta_d = 30^\circ$ after the immersion of the hydrociphher in water, as shown in Figure 3a. The reflectance signals

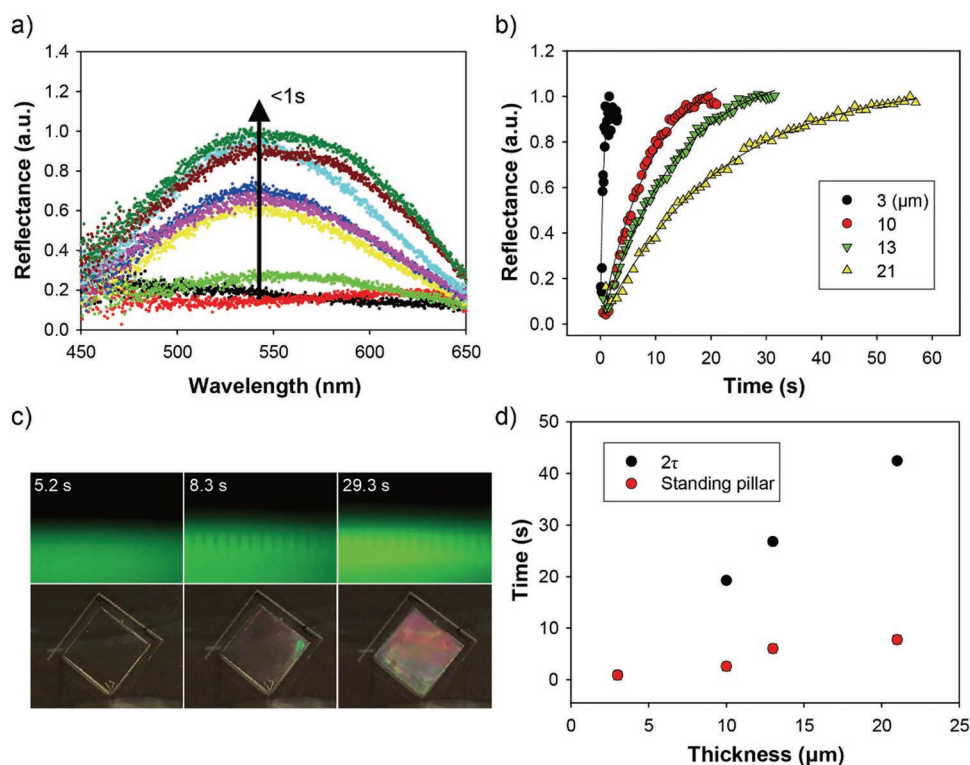


Figure 3. a) Temporal change in the reflectance spectrum for the 3 μm thick hydrogel-coated micropillar array after depositing water at a time interval of 0.1 s. b) Time-dependent reflectance (at the diffraction wavelength of 540 nm) of the hydrociphers with four different hydrogel thicknesses as denoted. The fitting results with the exponential equation are shown as solid lines. c) Time series of confocal microscope images showing the erection of micropillars (top) and images showing gradual coloration (bottom) for a 13.4 μm thick hydrociphher after depositing water. d) The optical response time (2τ) and the response time for the structural transformation (i.e., erection) of bent micropillars as a function of the hydrogel thickness.

centered at 540 nm were rapidly increased and saturated within a second. Considering the refractive index contrast, the recovery of the optical signal was completed when the hydrogel surrounding the micropillars was fully swollen with water. As the swelling of hydrogel is associated with the water diffusion through the composite film, the response time can be tuned by adjusting the thickness of the hydrogel layer. To verify this, the thickness of the dehydrated hydrogel layer was varied as 3, 10, 13, and 21 μm by varying the amount of the hydrogel precursors between the glass slide and the micropillar array, as shown in Figure S7 (Supporting Information). For all the four samples, the reflectance at 540 nm, $R(t)$, rapidly increased at the early stage and then gradually saturated, as shown in Figure 3b. These temporal changes can be depicted by an exponential function shown in Equation (2)

$$R(t) = R_0 [1 - \exp(-t/\tau)] \quad (2)$$

where R_0 is the maximum reflectance. By fitting the responses shown in Figure 3b with Equation (2), the characteristic time, τ , can be determined. The optical response time (2τ), at which 86.5% of the maximum reflectivity is recovered, was 0.9, 19, 27, and 42 s for 3, 10, 13, and 21 μm thick hydrociphers, respectively. This indicates that the reduction of the hydrogel layer thickness is critical for achieving fast colorization.

2.6. Revealing Mechanism for the Decryption

In consideration of the effect of the bent structure on the encryption of the structural color, the transformation from a bent to a straight structure upon hydration is a prerequisite to regain the structural color. To monitor the structural transformation, a dye-loaded micropillar array was prepared, and its dynamic reconfiguring process upon hydration was observed with a confocal microscopy. The epoxy resin containing a fluorescent dye of rhodamine B was used for the visualization. Although the individual micropillars in bent conformation were difficult to identify with the Z-stack confocal images, the evolution of the straightening reconfiguration during the hydration was clearly observed for the 13 μm thick hydrociphers, as shown in the top panels of Figure 3c and Movie S3 (Supporting Information).

With the transformation, the diffraction colors became more pronounced, as shown in the bottom panels of Figure 3c. It is noteworthy that the diffraction intensity increased further, even after the structural transformation was completed. The time required for the structural transformation, which was determined from the temporal changes of the confocal images, was 0.9, 2.6, 6.0, and 7.7 s for the 3, 10, 13, and 21 μm thick hydrociphers, respectively. For the 3 μm thick hydrociphers, the structural transformation time is comparable to its corresponding 2τ value (optical response time). However, for the thicker hydrogel layers, the structural transformation time was much shorter relative to its corresponding optical response time, as shown in Figure 3d. The result suggests that the erection of the micropillars was completed in the early stage of the hydration, which initiated the evolution of the diffraction color arising from the regular square array. As the hydrogel hydrated further, the increased refractive index contrast strengthened the diffraction intensity. This demonstrates that, as observed in the encryption process, both the structural effect and the refractive index effect were involved in the decryption process. For the 3 μm thick hydrociphers, the hydration process was fast enough to achieve a fully hydrated state within a second. The water sensitivity can be further improved by reducing the thickness of the hydrogel overcoat. For example, a 500 nm thick hydrogel-coated sub-micrometer pillar array disclosed the diffraction colors, even by exposure to exhaled humid air, as shown in Figure S8 and Movie S4 (Supporting Information). This showcases the facile tunability and customizability of the presented encryption platform for different application scenarios.

2.7. Reversibility of the Decryption and Encryption

The switching between the encrypted and decrypted states should be reversible and reliable over repetitive practical usage. We investigated the reflectivity changes of the 3 μm thick hydrociphers upon repeated cycling between the two states to assess the reversibility. For the ten repeated cycles, the reflectivity at 540 nm remained nearly unchanged for both hydrated and dehydrated states, as shown in Figure 4a. In addition, we measured the 2τ values upon the hydration for the ten cycles. The values were also invariant (0.92 ± 0.09) with the cycling, as

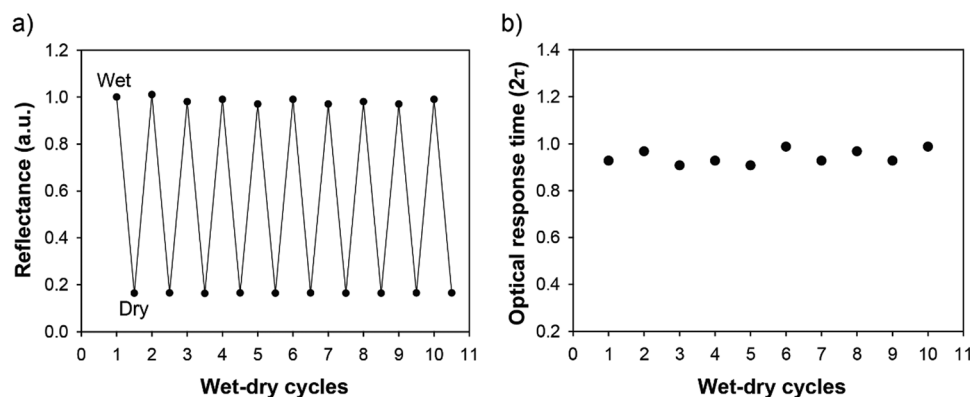


Figure 4. a,b) Change of reflectivity at the diffraction wavelength and optical response time (2τ) for reflectivity change by hydration during ten cycles of hydration and drying.

shown in Figure 4b. This high reversibility can be attributed to the covalent bonds between the micropillars and hydrogel layer, which withstands the stress at the hydrogel/micropillar interface generated by the volume change of the surrounding hydrogel.^[13]

3. Conclusion

In this work, we developed a “hydrocipher” based on a hydrogel-coated micropillar array, whose diffraction colors can be reversibly switched on by hydration and off by drying, as a cryptographic technique for advanced security and general anti-counterfeit applications. By using the in situ synthesis of the water-swollen PAAm gel on the micropillar array, the hydrated hydrogel-coated micropillar array, which exhibits an iridescent structural color, was successfully fabricated. With the dehydration of the hydrogel, the film encrypted the color patterns due to the combined effect of the refractive index change of the hydrogel and the bending of the micropillars. In the encrypted state, the dehydrated hydrogel effectively protected the delicate micropillar structures from external mechanical stress, which prevents potential damage of grating structure from dust in ambient environment in practical usage. The color patterns were quickly decrypted in a second by liquid water swelling or exposing to humid air. The encryption/decryption process was highly reversible due to the high physical integrity of the hydrogel and micropillars via covalent bonds. With the merits of complete encryption and fast decryption, high robustness, and long-lasting durability as well as the scalable fabrication, we believe our water-responsive reconfigurable diffraction grating can potentially serve as a practical platform as a user-interactive cryptographic tag, for message authentication coding and general anti-counterfeiting applications.

4. Experimental Section

Preparation of PDMS Molds: Silicon masters containing the cylindrical micropillar arrays were fabricated using the photolithography process. The micropillars had a diameter of 1 μm and a height of 3 μm , and their square array had a period of 2 μm . The surface of the silicon master was coated with 1H,1H,2H,2H-perfluorodecyltriethoxysilane (Alfa Aesar) by incubating the master with a dish containing the silane under vacuum in a desiccator at room temperature for 6 h. This chemical treatment facilitated the release of PDMS from the master. A mixture of a prepolymer and a crosslinker (Sylgard 184, Dow Corning, Midland, MI) at a weight ratio of 10:1 was degassed under vacuum, which was then gently poured on the surface-treated master. After curing PDMS at 70 $^{\circ}\text{C}$ for 2 h, the resulting PDMS mold was peeled off from the master.

Preparation of Patterned PDMS Molds: Glass substrates were cleaned by ultrasonication in acetone and ethanol, respectively, and oxygen-plasma treatment. The glass substrates were immersed in the mixture of 3-(trimethoxysilyl) propyl methacrylate (TMSPMA, Sigma-Aldrich), ethanol, and 10% acetic acid in a volume ratio of 1:100:3 for 12 h. The substrates were washed with ethanol and completely dried by air-blowing. A drop of the epoxy resin (PB126616) containing 1 wt% glycidyl methacrylate (Sigma-Aldrich) was deposited onto the silanized glass substrate, on which the PDMS mold was placed. After the complete filling of cylindrical holes in the PDMS mold with the epoxy resin for 5 min, a photomask was placed on the PDMS mold. In addition, a collimated UV laser with a wavelength of 325 nm and an intensity of 4.2 mW cm^{-2} was irradiated for 2 min through the photomask. After the release of the mold, the uncured epoxy at the surrounding was flattened,

which was irradiated by a UV lamp with a wavelength range of 320–390 nm (Dymax 5000-EC) with an intensity of 400 W. The pattern of the epoxy mold was then replicated to PDMS by following the same protocol for the preparation of the PDMS mold described above.

Production of Hydrogel-Coated Micropillar Array: By following the same procedure for the preparation of the patterned PDMS mold, a patterned micropillar array was formed on either the glass or on the PET substrates, where no photomask was used. To make a hydrogel layer, an aqueous solution of 10 w/w% acrylamide, 1 w/w% N,N'-methylenebis(acrylamide), and 0.5 w/w% 2-hydroxy-4'-(2-hydroxyethoxy)-2-methylpropiophenone was deposited on the surface of the micropillar array, where the volume of the precursor solution was adjusted to 25, 50, 75, and 100 μL to set the thicknesses of 3, 10, 13, and 21 μm , respectively. The chemical structures of the hydrogel monomers and polymer and the FTIR result of the polymer are shown in Figure S9 (Supporting Information). The precursor was covered by a slide glass with an area of $2.2 \times 2.2 \text{ cm}^2$ and irradiated by a UV lamp (Dymax 5000-EC) for 1 min. Finally, the slide glass was gently detached from the hydrogel layer. For drying hydrogel, the hydrocipher was kept at room temperature for about 30 min, where the complete dehydration is confirmed by weight scale measurement and thermogravimetric analysis as shown in Figure S10 (Supporting Information).

Characterization: The top surface of hydrogel-free micropillar arrays and cross section of hydrogel-coated micropillar arrays were observed with a SEM (SM-701, TOPCON) at 10 keV after sputter-coating with 10 \AA platinum. To directly observe the dynamic transformation of micropillars, the micropillars were prepared using the epoxy resin containing 1 w/w% fluorescent dye (rhodamine B, Sigma-Aldrich) and observed with a confocal microscopy (Leica DMI3000 SP5 TCS). The reflection spectra were measured using a fiber-coupled spectrometer (Ocean Optics Inc., USB 4000), and the transmission spectra were measured using a UV-vis spectrometer (GENESYS 10S). The FTIR analysis was conducted using JASCO Model 420 FTIR using a potassium bromide (KBr) pellet. FTIR spectra were recorded in the spectral range of $4000\text{--}400 \text{ cm}^{-1}$ with a 2 cm^{-1} resolution and 32 scans.

Supporting Information

Supporting Information is available from the Wiley Online Library or from the author.

Acknowledgements

J.C. and M.H. contributed equally to this work. This work was supported by the KAIST Institute for the Nano-Century, the Korea Institute of Energy Technology Evaluation and Planning (KETEP) and the Ministry of Trade, Industry & Energy (MOTIE) of the Republic of Korea (No. 20173010032100), the NSF CAREER Award 1724526, the ONR Award N000141712117, the ONR Award N00014-18-1-2314, the AFOSR award FA9550-17-1-0311, the AFOSR award FA9550-18-1-0449, and the Hellman Fellows Funds.

Conflict of Interest

The authors declare no conflict of interest.

Keywords

2D gratings, anti-counterfeit tags, hydrogels, micropillars, structural colors

Received: July 25, 2019
Revised: October 3, 2019
Published online:

- [1] a) J. Ge, Y. Yin, *Angew. Chem., Int. Ed.* **2011**, *50*, 1492; b) P. Jiang, J. F. Bertone, K. S. Hwang, V. L. Colvin, *Chem. Mater.* **1999**, *11*, 2132.
- [2] a) Y. Zhao, Z. Xie, H. Gu, C. Zhu, Z. Gu, *Chem. Soc. Rev.* **2012**, *41*, 3297; b) I. B. Burgess, M. Lončar, J. Aizenberg, *J. Mater. Chem. C* **2013**, *1*, 6075; c) T. Lu, H. Pan, J. Ma, Y. Li, S. Bokhari, X. Jiang, S. Zhu, D. Zhang, *ACS Appl. Mater. Interfaces* **2017**, *9*, 18231; d) E. Tian, J. Wang, Y. Zheng, Y. Song, L. Jiang, D. Zhu, *J. Mater. Chem.* **2008**, *18*, 1116.
- [3] a) S. Cho, T. S. Shim, J. H. Kim, D.-H. Kim, S.-H. Kim, *Adv. Mater.* **2017**, *29*, 1700256; b) M. Qin, M. Sun, R. Bai, Y. Mao, X. Qian, D. Sikka, Y. Zhao, H. J. Qi, Z. Suo, X. He, *Adv. Mater.* **2018**, *30*, 1800468; c) M. Qin, M. Sun, M. Hua, X. He, *Curr. Opin. Solid State Mater. Sci.* **2019**, *23*, 13; d) M. Sun, R. Bai, X. Yang, J. Song, M. Qin, Z. Suo, X. He, *Adv. Mater.* **2018**, *30*, 1804916.
- [4] a) H. S. Lee, T. S. Shim, H. Hwang, S.-M. Yang, S.-H. Kim, *Chem. Mater.* **2013**, *25*, 2684; b) Y. Heo, S. Y. Lee, J.-W. Kim, T. Y. Jeon, S.-H. Kim, *ACS Appl. Mater. Interfaces* **2017**, *9*, 43098.
- [5] a) T. Ding, G. Cao, C. G. Schäfer, Q. Zhao, M. Gallei, S. K. Smoukov, J. J. Baumberg, *ACS Appl. Mater. Interfaces* **2015**, *7*, 13497; b) A. Harris, *Orgalime Guide Combating Counterfeiting: A Practical Guide for European Engineering Companies*, Orgalime, Schaerbeek, Brussels, Belgium **2001**.
- [6] a) S. Ye, Q. Fu, J. Ge, *Adv. Funct. Mater.* **2014**, *24*, 6430; b) S. Ye, J. Ge, *J. Mater. Chem. C* **2015**, *3*, 8097; c) R. Xuan, J. Ge, *J. Mater. Chem.* **2012**, *22*, 367.
- [7] a) M. Moirangthem, A. P. H. J. Schenning, *ACS Appl. Mater. Interfaces* **2018**, *10*, 4168; b) M. K. Khan, A. Bsoul, K. Walus, W. Y. Hamad, M. J. MacLachlan, *Angew. Chem., Int. Ed.* **2015**, *54*, 4304.
- [8] a) K. Zhong, J. Li, L. Liu, S. Van Cleuvenbergen, K. Song, K. Clays, *Adv. Mater.* **2018**, *30*, 1707246; b) I. B. Burgess, L. Mishchenko, B. D. Hatton, M. Kolle, M. Lončar, J. Aizenberg, *J. Am. Chem. Soc.* **2011**, *133*, 12430; c) Y. Heo, H. Kang, J.-S. Lee, Y.-K. Oh, S.-H. Kim, *Small* **2016**, *12*, 3819.
- [9] a) Y. Qi, L. Chu, W. Niu, B. Tang, S. Wu, W. Ma, S. Zhang, *Adv. Funct. Mater.* **2019**, *29*, 1903743; b) Y. Meng, J. Qiu, S. Wu, B. Ju, S. Zhang, B. Tang, *ACS Appl. Mater. Interfaces* **2018**, *10*, 38459.
- [10] a) H. Nam, K. Song, D. Ha, T. Kim, *Sci. Rep.* **2016**, *6*, 30885; b) H. Ma, Y. Tan, J. Cao, S. C. Lian, K. Chen, W. Luo, J. Guan, *J. Mater. Chem. C* **2018**, *6*, 4531; c) W. Luo, Q. Cui, K. Fang, K. Chem, H. Ma, J. Guan, *Nano Lett.* **2018**, <https://doi.org/10.1021/acs.nanolett.7b04218>.
- [11] G. Si, Y. Zhao, E. S. P. Leong, J. Lv, Y. J. Liu, *Nanotechnology* **2014**, *25*, 455203.
- [12] a) J. Ge, H. Lee, L. He, J. Kim, Z. Lu, H. Kim, J. Geobl, S. Kwon, Y. Yin, *J. Am. Chem. Soc.* **2009**, *131*, 15687; b) R. Xuan, J. Ge, *Langmuir* **2011**, *27*, 5694.
- [13] J. Choi, W. Cho, Y. S. Jung, H. S. Kang, H.-T. Kim, *ACS Nano* **2017**, *11*, 1320.
- [14] E. L. Prime, D. H. Solomon, *Angew. Chem., Int. Ed.* **2010**, *49*, 3726.
- [15] C.-Y. Peng, C.-W. Hsu, C.-W. Li, P.-L. Wang, C.-C. Jeng, C.-C. Chang, G.-J. Wang, *ACS Appl. Mater. Interfaces* **2018**, *10*, 9858.
- [16] a) A. Sidorenko, T. Krupenkin, A. Taylor, P. Fratzl, J. Aizenberg, *Science* **2007**, *315*, 487; b) B. Pokroy, S. H. Kang, L. Mahadevan, J. Aizenberg, *Science* **2009**, *323*, 237; c) X. He, M. Aizenberg, O. Kuksenok, L. D. Zarzar, A. Shastri, A. C. Balazs, J. Aizenberg, *Nature* **2012**, *487*, 214; d) A. Shastri, L. M. McGregor, Y. Liu, V. Harris, H. Nan, M. Mujica, Y. Vasquez, A. Bhattacharya, Y. Ma, M. Aizenberg, O. Kuksenok, A. C. Balazs, J. Aizenberg, X. He, *Nat. Chem.* **2015**, *7*, 447.
- [17] C. Zhou, D. E. Heath, A. R. M. Sharif, S. Rayatpisheh, B. H. L. Oh, X. Rong, R. Beuerman, M. B. Chan-Park, *Macromol. Biosci.* **2013**, *13*, 1485.
- [18] A. M. Nastas, M. S. Iovu, *Tech. Phys.* **2015**, *60*, 464.
- [19] E. Lee, M. Zhang, Y. Cho, Y. Cui, J. Van der Spiegel, N. Engheta, S. Yang, *Adv. Mater.* **2014**, *26*, 4127.
- [20] K. Hara, A. Nakamura, N. Hiramatsu, A. Matsumoto, *Jpn. J. Appl. Phys.* **2000**, *39*, 2913.
- [21] a) Poly(acrylamide) Properties, <https://polymerdatabase.com/polymers/polyacrylamide.html> (accessed: June 2019); b) Polyacrylamide Properties, https://www.chemicalbook.com/Chemical-ProductProperty_EN_CB7390058.htm (accessed: June 2019).